Convective and Stratiform Precipitation Processes and their Relationship to Latent Heating

Wei-Kuo Tao, Steve Lang, Xiping Zeng
Shoichi Shige and Yukari Takayabu

Submitted to the *J. Climate*

Popular Summary

The global hydrological cycle is central to the Earth's climate system, with rainfall and the physics of its formation acting as the key links in the cycle. Two-thirds of global rainfall occurs in the Tropics. Associated with this rainfall is a vast amount of heat, which is known as latent heat. It arises mainly due to the phase change of water vapor condensing into liquid droplets; three-fourths of the total heat energy available to the Earth's atmosphere comes from tropical rainfall. In addition, fresh water provided by tropical rainfall and its variability exerts a large impact upon the structure and motions of the upper ocean layer.

An improved convective -stratiform heating (CSH) algorithm has been developed to obtain the 3D structure of cloud heating over the Tropics based on two sources of information: 1) rainfall information, namely its amount and the fraction due to light rain intensity, observed directly from the Precipitation Radar (PR) on board the TRMM satellite and 2) synthetic cloud physics information obtained from cloud-resolving model (CRM) simulations of cloud systems. The cloud simulations provide details on cloud processes, specifically latent heating, eddy heat flux convergence and radiative heating/cooling, that are not directly observable by satellite. The new CSH algorithm-derived heating has a noticeably different heating structure over both ocean and land regions compared to the previous CSH algorithm. One of the major differences between new and old algorithms is that the level of maximum cloud heating occurs 1 to 1.5 km lower in the atmosphere in the new algorithm. This can effect the structure of the implied air currents associated with the general circulation of the atmosphere in the Tropics.

The new CSH algorithm will be used provide retrieved heating data to other heating algorithms to supplement their performance.

Convective and Stratiform Precipitation Processes and their Relationship to Latent Heating

Wei-Kuo Tao[1], Steve Lang[1,2], Xiping Zeng[1,3]
Shoichi Shige[4] and Yukari Takayabu[5]

[1]*Laboratory for Atmospheres*
NASA/Goddard Space Flight Center
Greenbelt, MD 20771, USA

[2]*Science Systems and Applications Inc.*
Lanham, MD 20706, USA

[3]*Goddard Earth Sciences and Technology Center*
University of Maryland, Baltimore County
Baltimore, 21250, MD, USA

[4]*Dept. of Aerospace Engineering*
Osaka Prefecture University
Sakai, Osaka 599-8531, Japan

[5]*Center for Climate System Research*
University of Tokyo
Tokyo 153-8904, Japan

J. Climate

Submitted to TRMM LH Special Collection

Corresponding author address: Dr. W.-K. Tao, Laboratory for Atmosphere, NASA/GSFC, Greenbelt, MD 20771
Wei-Kuo Tao <Wei-Kuo.Tao-1@nasa.gov>

Abstract

The relationship between the surface rainfall intensity and its associated stratiform amount is investigated by examining the Tropical Rainfall Measurement Mission (TRMM) Precipitation Radar (PR) product and the Cloud Resolving Model (CRM) simulated precipitation data. The results showed that there are more stratiform rain amount for light rain for both ocean and land region, but more convective rain amount for heavy rainfall. The differences between oceanic and land region is that more convective rain for precipitation rate over 100 mm/day for the land region than its oceanic counterpart.

An improved convective –stratiform heating (CSH) algorithm is developed based on the PR rainfall product (rainfall intensity and stratiform percentage) and CRM simulated latent heating, eddy convergence/divergence and radiative heating/cooling. The new CSH algorithm derived heating has very different heating structure for the ocean and land regions compared to previous CSH algorithm derived. Another major difference between new and previous CSH algorithm is that the level of maximum heating is 1 to 1.5 km lower for the new than old CSH algorithm.

1. Introduction

Latent heat is dominated by phase changes between water vapor and small liquid or frozen cloud-sized particles. It consists of condensation of cloud droplets, evaporation of cloud droplets and raindrops, freezing of raindrops, melting of snow and graupel/hail, and the deposition and sublimation of ice particles. In addition, eddy heat flux convergence from cloud motions can also result in distributing the heating or cooling vertically and horizontally. Latent heating cannot be measured directly with current techniques. These processes are not directly detectable with current remote sensing or *in situ* instruments, which explain why the retrieval schemes to be discussed depend heavily on some type of cloud-resolving model (CRM). But, it can be derived indirectly by measuring the vertical profiles of temperature and the 3D wind fields from extensive rawinsonde networks through a residual method (called a diagnostic budget; Yanai *et al.* 1973; House 1982, 1997; Johnson 1984, Zhang and Lin 1997, Schumacher *et al.* 2006).

The launch of the Tropical Rainfall Measuring Mission (TRMM) satellite, a joint U.S.-Japan project, in November of 1997 made it possible for quantitative measurements of tropical rainfall to be obtained on a continuous basis over the entire global tropics. TRMM provides a much needed and accurate measurement of rainfall as well as an estimate of the four-dimensional structure of latent (diabatic) heating over the global tropics. In the last few years, it has been established that standard products of LH from TRMM measurements would be a valuable resource for scientific research and applications (see a review by Tao *et al.* 2006). Such products would enable new insights and investigations concerning the complexities of convection system life cycles, the diabatic heating controls and feedbacks

related to meso-synoptic circulations and their forecasting, the relationship of tropical patterns of LH to the global circulation and climate, and strategies for improving cloud parameterizations in environmental prediction models.

Five different TRMM LH algorithms designed for applications with satellite-estimated surface rain rate and precipitation profile inputs have been developed, intercompared, validated, and applied in the past decade (see Tao *et al.* 2006; 2007). They are the: (1) Goddard Convective-Stratiform Heating (CSH) algorithm, (2) Hydrometeor Heating (HH) algorithm, (3) Goddard Profiling Heating (GPROF Heating) algorithm, (4) Spectral Latent Heating (SLH) algorithm, and (5) Precipitation Radar Heating (PRH) algorithm. The CSH algorithm only requires information on the surface precipitation rates, amount of stratiform rain, and the type and location of the observed cloud systems (Tao *et al.* 1993). A lookup table, however, is used containing stored convective and stratiform latent heating profiles, normalized by total surface rain rates, for various types of cloud systems in different geographic locations. These profiles are mostly obtained from CRM (GCE model) simulations. In GPROF, CRM-simulated hydrometeor and associated latent heating vertical profiles that have radiative characteristics consistent with a given set of multi-spectral microwave radiometric observations are composited to create (retrieve) a best estimate of the observed profiles (Olson *et al.* 1999, Grecu *et al.* 2009). The HH and algorithm[1] estimates latent heating profiles as a function of the vertical derivative of the retrieved hydrometeor profiles (Yang and Smith 1999). The derivation and evaluation of the HH algorithm is also based on CRM simulations. It requires information about the vertical profiles of cloud- and

[1] Tao *et al.* (1990) were the first to put forth a latent heating algorithm that was termed a hydrometeor/heating algorithm. Tao *et al.* (1993) then improved the performance of the HH algorithm by including surface rain rates.

precipitation-sized water and ice particles, all of which can be obtained from the TMI profiler retrievals (Smith *et al.* 1992, 1994). The terminal (fall) velocities of the large cloud (precipitating) particles (rain, snow and graupel/hail) are also required for the HH algorithm. Cloud-scale velocity is needed in Yang and Smith (1999a,b) and is obtained by applying a regression method to a CRM-simulated database. The SLH algorithm (Shige *et al.* 2004, 2006, 2009) is also based on GCE model results. It uses PR information (melting layer, precipitation top height, rain rate and type) to select the heating profiles in a look-up table. The PRH algorithm (Satoh and Noda 2001, Katsumata *et al.* 2009) also uses PR information but without using any heating profiles simulated by CRMs. However, it needs to estimate the cloud drafts and (standard) thermodynamic structures associated with cloud systems. An iteration calculation is applied to match the relationship between rainfall and latent heating. The strengths and weaknesses of each algorithm were discussed in Tao *et al.* (2006). Table 1 lists the data required, heating product of each algorithm and key references of these algorithms.

In this paper, both TRMM PR and CRM simulated results will be used to examine and quantify the convective and stratiform percentage and their relationship with surface rainfall and latent heating for convective systems that developed in different geographic locations. The results from the GCE model simulations will be used to calculate the each components of atmospheric budget (latent heat. eddy transport and radiation). These simulated results will be used for the improvement of a new CSH algorithm. In Section 2, the model and model set-up used, and cases are described. The results are shown and discussed in Section 3. In section 4, the performance of new CSH algorithm will be presented. Finally, the major results and future work are summarized in Section 5.

2. Numerical Modeling and Data

2.1 Goddard Cumulus Ensemble (GCE) Model

The Goddard Cumulus Ensemble (GCE) model, a Cloud Resolving Model (CRM), is used to simulate clouds/cloud systems and their associated heating budget. It is non-hydrostatic. It takes account of both the absorption and scattering for solar radiation and both the emission and absorption for infrared radiation. Its cloud-radiation interaction has been assessed (Tao *et al*. 1996; 2003). Subgrid-scale (turbulent) processes in the model are parameterized using a scheme based on Klemp and Wilhelmson (1978) and Soong and Ogura (1980). The effects of both dry and moist processes on the generation of subgrid-scale kinetic energy have been incorporated. The sedimentation of cloud ice (Starr and Cox 1985) is included to better model clouds in the upper troposphere. All scalar variables (temperature, water vapor, and all hydrometeors) are calculated with a positive definite advection scheme (Smolarkiewicz and Grabowski 1990). Results from the positive definite advection scheme are in better agreement with observations for tropical cloud systems (Johnson *et al*. 2002).

The model has five prognostic hydrometeor variables: the mixing ratios of cloud water, rainwater, cloud ice, snow and graupel. It has recently modified by Lang *et al.* (2007) to reduce un-realistic large precipitating ice particles and by Zeng *et al.* (2008, 2009) to introduce the ice nuclei concentration into the parameterization of the Bergeron process as an input factor. The development and main features of the GCE model were also published in Tao and Simpson (1993) and Tao *et al.* (2003). A review on the application of the GCE

model to better understand precipitation processes can be found in Simpson and Tao (1993) and Tao (2002).

In the GCE model, each grid point is designated as either a cloudy or clear area for each integration time, depending upon whether the sum of the cloud water and ice mixing ratios are larger than 10^{-3} (or 10^{-5} depending on the type of clouds/cloud systems) g/kg at each grid point (usually an indicator of 100% relative humidity). In the cloudy area, each grid point can also be designated as either being in the active or non-active updraft or downdraft region (Tao *et al.* 1987). In addition, the cloud characteristics can be divided into convective and stratiform components (Tao *et al.* 1993; Lang *et al.* 2003). In short, convective regions include those with large vertical velocities (exceeding 3-5 m s^{-1}) and/or large surface precipitation rates. The stratiform region is separated into regions with or without surface rainfall.

The model in the present paper has the same structure as that in previous studies (e.g., Soong and Tao 1980; Tao and Soong 1986; Johnson *et al*. 2002; Tao *et al.* 2003; 2004; Zeng *et al*. 2007 and many others) wherein clouds are simulated under prescribed large-scale forcing. The default numerical experiment is two-dimensional, using a 1 km horizontal resolution and vertical resolution that ranges from 42.5 m at the bottom to 1 km at the model top, which is at 22.5 km. The model uses a time step of 6 seconds and 512x41 grid points for integration. Please see more details in Zeng *et al.* (2008, 2009).

2.2 Data

(a) Oceanic Convective Systems (GATE, TOGA COARE and SCSMEX)

The South China Sea Monsoon Experiment (SCSMEX) was conducted in May-June 1998. Two major convective events, prior to and during monsoon onset (May 18-26, 1998) and post monsoon (June 2-11, 1998) are observed. The SCSMEX forcing data were obtained from a variational analysis approach (Zhang and Lin 1997; Zhang *et al*. 2001). Its numerical simulation starts at 0600 UTC 6 May 1998 and lasts for 44 days. The Tropical Oceans Global Atmosphere (TOGA) - Coupled Ocean Atmosphere Response Experiment (COARE) was conducted in 1992 and 1993 over the Central Pacific. The most intense convection during TOGA COARE occurred in middle and late December 1992, prior to the peak of westerly wind bursts around 1 January 1993. Several major convective events occurred around 11-16 and 20-25 December 1992, mainly due to low-level large-scale convergence of easterlies and westerliey (Lin and Johnson 1996). For TOGA COARE, the large-scale forcing used in the GCE model was derived from Intensive Flux Array (UFA) sounding networks (Lin and Johnson 1996). GARP (Global Atmospheric Research Program) Atlantic Tropical Experiment (GATE) was conducted in 1974 over East Atlantic. Cloud systems (non-squall clusters, a squall line, and scattered convection) for the period 1-8 September 1974 phase III of GATE have also been simulated using the GCE model (Li *et al.* 1999; Tao 2003). Sui and Yanai (1986) provided the GATE large-scale forcing for the GCE model. The environmental conditions for SCSMEX, TOGA COARE and GATE can be found in Tao *et al.* (2004). A TOGA-COARE surface flux algorithm (Wang *et al.* 1996) is used to calculate sea surface fluxes for these oceanic cases.

(b) Continental Cases (ARM 1997 and 2002)

The Atmospheric Radiation Measurement (ARM) program set up the Southern Great Plains (SGP) site to observe clouds and precipitation for climate research. The site was centered at 36.6°N and 96.5°W. Two field campaigns at the site, conducted in summers of 1997 and 2002, are referred to here as ARM-SGP-97 and 02. The ARM forcing data were also obtained from the variational analysis approach of Zhang and Lin (1997) and Zhang *et al.* (2001). The surface fluxes are obtained from site-wide averages of observed fluxes from the ARM Energy Balance Bowen Ratio (EBBR) stations and are used to drive the model (Zeng *et al.* 2007). The ARM-SGP-97 numerical simulation starts at 2330 UTC 18 June 1997 and lasts for 29 days. The ARM-SGP-02 one starts at 2030 UTC 25 May 2002 and lasts for 20 days. For the ARM cases, the surface fluxes are prescribed, and the surface wind does not interact with the boundary layer.

All SCSMEX, TOGA COARE, GATE, ARM cases were simulated by GCE model previously. Please refer to Das *et al.* (1999). Li *et al.* (1999) and Zeng *et al.* (2009), for GATE, Johnson *et al.* (2002) and Zeng *et al.* (2009) for the TOGA COARE cases, Tao *et al.* (2003b) and Zeng *et al.* (2008) for the SCSMEX cases and Xu *et al.* (2002), Zeng *et al.* (2007, 2009) for the ARM cases with regard to the temporal variation of the wind shear. Table 2 summarizes all GCE model integrations for these cases.

2.3 TRMM PR

The TRMM Precipitation Radar (PR) operates at a frequency 13.8 GHz. This is a moderately attenuating frequency so that one of the major objectives of the PR algorithms is

to estimate and correct for the path attenuation. Because the PR is a single-wavelength, single-polarization, non-Doppler radar, there are only a few methods available to estimate rainfall. These include the Hitschfeld-Bordan (HB) method, the surface reference technique or SRT, a "hybrid" of these, and the mirror-image technique. The rain estimation algorithm uses a hybrid of the Hitschfeld-Bordan method and the SRT to correct for attenuation and derive an estimate of the range profile of the radar reflectivity factor, dBZ. The rain rate profile is then calculated from the dBZ profile and an appropriate Z-R relationship. The algorithm also includes surface clutter rejection and an attempt to correct for effects of non-uniform beam filling.

Convective-stratiform classification of the rain is based on a combination of the vertical and horizontal structure of the radar reflectivity field. The vertical profile is checked for the presence of a bright-band (melting layer) by considering the behavior of the second derivative of the radar range profile. When the second derivative exceeds a threshold, a bright band is taken to be present and the rain is classified as stratiform. In cases where a clearly defined melting layer is absent, the horizontal rain structure is examined by means of a modified version of an algorithm designed for the analysis of ground-based radar data.

Statistics of the instantaneous, high-resolution rain rates are compiled on a monthly basis over 0.5^{o} x 0.5^{o} latitude-longitude grids. Near-surface rain rates and the rain rates at 3 altitude levels are stored according to rain type. The statistics include means, standard deviations and histograms of the rain rate, radar reflectivity factors, bright-band and storm heights.

3. Results

3.1 PR estimated relationship between rainfall intensity and stratiform percentage

Figure 1 shows the relationship between rainfall intensity and stratiform precipitation percentage for ocean and land region from PR. The difference between two regions is not significant. For example, there are more stratiform rain amount (percentage) for light rain (intensity) from 10 to 120 mm/day (or less than 1 mm/hour to 5 mm/hour) for both ocean and land region, but more convective rain amount for heavy rainfall (over 200 mm/day). This result might imply that there is general relationship between rainfall intensity and startiform amount. It also suggests that convective – stratiform heating algorithm could use this relationship to build its look-up heating table (more discussion in section 4). However, there are differences between oceanic and land region that showed in the low stratiform (or high convective) regime. For example, more convective rain for precipitation rate over 100 mm/day for the land region than its oceanic counterpart.

Figure 2 shows TRMM PR observed relationship between rainfall intensity and stratiform precipitation percentage over SCSMEX / NESA for May – June of 1998. It also shows the same SCSMEX region and the same period but for 10 years of observation. Again, the light (heavy) rainfall regime shows more (less) stratiform rainfall amount. Since SCSMEX / NESA region is where monsoon occurs and that may explain the more convective rain amount for heavy rainfall (similar to land as shown in Fig. 1(a)). Table 3 shows PR observed rainfall amount and stratiform percentage for global tropics (52.8%) and its oceanic (55.0%) and continental (47,4%) components. More stratiform amount (about 7%

difference) was observed for oceanic than continental convection. Similar result also found in regional (SCSMEX-monsoon and ARM region). More stratiform rain amount occurs for SCSMEX than ARM cases.

Schumacher and Houze (2003) examined the stratiform rain in the tropics using TRMM PR. Their results showed that stratiform accounts for 40% of total rain amount over 20° N to 20° S for 3-year period (1998-2000). Their results also showed that convective rain rates attain greater value over land (from 26 to 38%) than ocean (from 41 to 53%) regions. In addition, their results found that 53% (36%) of stratiform rain amount occurs over Southeast Pacific (South and North America). Generally, these conclusions are good agreement with our results that are based on 10-year period of TRMM PR and over larger geographic area, except that more global tropic stratiform amount was shown in our results.

3.2 GCE model simulated relationship between rainfall intensity and stratiform percentage

In order to compare the TRMM 0.5 x 0.5 degree rainfall products, the GCE model simulated results were divided the domain (512 km) equally into 8 sub-domains so that each has a horizontal scale of 64 km. Then, average rainfall rates/amounts in convective and stratiform regions (including its percentage to total rainfall) in each sub-domain were calculated. Using the stratiform percentage and the average rate, the sub-domain is classified to be an element of a 36x20-size array, where the array has a precipitation rate interval of 20 mm/day (about 1 mm/hour) and a stratiform percentage interval of 5%. Finally, calculate the vertical distributions of heating in each sub-domain and over the entire modeling period.

Figure 3 shows the model simulated PDF of the relationship between rainfall intensity and startiform percentage over land and ocean regions. For oceanic region, a total of 123 day model integration combining SCSMEX, TOGA COARE and GATE cases. Shorter model integration for ARM cases (a total of 49 days by combining 1997 and 2002) was for land region. That is why a smother PDF was shown in the oceanic case. The model results also show similar feature as in PR observation (Fig. 1). For example, there is more stratiform rain amount (percentage) for light rain (intensity) from 10 to 120 mm/day (or less than 1 mm/hour to 5 mm/hour) for both ocean and land region, but more convective rain amount for heavy rainfall (over 200 mm/day) for land case. However, there is one major difference between PR observation and model simulation that is model simulates high stratiform rain amount for very small rainfall case (10 mm/day or < 1 mm/hour). The sensitivity of PR for not detecting very light rain (17 dBz) is the main reason for this difference.

Figure 4 shows the relationship between rainfall intensity and startiform percentage for each individual land and ocean case. Clearly, the two summer land cases (or ARM 1997 and ARM 2002) show similar behavior in terms of more convective rain for high rainfall intensity just as the oceanic cases. In addition, the land cases have higher frequency in heavy rainfall rate and small stratiform percentage than the oceanic ones, which is consistent with the observations shown in Fig. 1.

Table 4 shows grid-averaged total rainfall and stratiform percentage for GCE simulated cases. More rainfall is occurred in the oceanic cases than those of continental cases. This is due to the fact that more precipitable water (or moist) in oceanic environment

than its continental counterpart (see Table 1 in Tao *et al.* 2004). The vertically integrated water vapor contents are very moist for the SCSMEX cases (over 62 g cm^{-2}) compared to the TOGA COARE and GATE cases. That is the reason for largest rainfall for SCSMEX simulation. For TOGA COARE and GATE cases, the environmental condition is more moisten in TOGA COARE but with less rainfall amount than GATE. It is because that the model simulation starts in November that did not have many active convective events. Generally speaking, more stratiform percentage (40-50%) should be simulated in the tropical oceanic cases than mid latitude continental cases. However, the ARM cases also have large stratiform rain amount/percentage (from 36 to 41%). Houze (1977), Zipser *et al.* (1981) and Gamache and Houze (1983) estimated that the widespread stratiform rain accounted for about 32%-49% of the total rainfall from the GATE cases. The fraction of stratiform rainfall from midlatitude squall lines has been estimated at 29%-43% (Rutledge and Houze 1987; Johnson and Hamilton 1988). The GCE model simulated results are in good agreement with these observations.

By comparing GCE model simulation and PR observations (Table 2), the simulated rainfall amount for ARM (2002) case is much larger than the PR estimated. The sampling may be the reason for this difference. On the other hand, the GCE model simulated stratiform percentage for SCSMEX and ARM (2002) cases are in excellent agreement with TRMM PR estimated. In addition, the GCE model simulated rainfall amounts for SCSMEX, ARM (1997 and 2002) and GATE cases are in good agreement with those estimated by sounding networks. The TOGA COARE case is 17% less than sounding estimated. The GCE model has simulated two TOGA COARE cases (10-17 December 1992 and 19-27 December 1992) and the simulated rainfall is an excellent agreement with sounding

estimated (see Table 5 in Tao *et al.* 2004). We believe that the difference mainly occurs during the November 1992 model integration.

3.3 GCE model simulated each component of heating budget

Q_1 can directly relate to the contributions of cloud effects which can be explicitly estimated by GCE model (Soong and Tao 1980; Tao and Soong 1986; Tao *et al.* 1993a and many others):

$$Q_1 = \bar{\pi}[-\frac{\partial \bar{\rho} w'\theta'}{\bar{\rho}\partial z} - \nabla \bullet V\theta'] + \frac{1}{c_p}[L_v(c-e) + L_f(f-m) + L_s(d-s)] + Q_R \qquad (1)$$

where the primes indicate deviations from the large-scale environment mainly due to small scale cloud processes. The variable θ is potential temperature; ρ is air density; $\bar{\pi} = (p / P_{oo})^{R/c_p}$ is non-dimensional pressure (where p and p_{oo} are dimensional and reference pressures with p_{oo} taken as 1000 hPa), and c_p and R represent the specific heat at constant pressure and the gas constant of dry air, respectively. The variables L_v, L_f, and L_s are the latent heats of condensation, freezing, and sublimation, respectively, while the variables (c, e, f, m, d, s) denote rates for condensation of cloud droplets, evaporation of cloud droplets and rain drops, freezing of water droplets and rain drops, melting of ice crystals, snow flakes, graupel and hail, deposition of ice crystals, and sublimation of all ice hydrometeors, respectively.

The term $(1/c_p)\ [L_v(c-e) + L_f(f-m) + L_s(d-s)]$ is the LH due to microphysical phase changes. As defined in Yanai *et al.* (1973), Q_1 is the apparent heat source, while Q_R is

the radiative heating/cooling rate associated with radiative transfer processes. The first two terms on the right-hand side of Eq. (1) are the vertical and horizontal eddy heat flux convergence ($\overline{\pi}[\overline{\partial w'\theta'/\partial z}]$ and $\overline{\pi}[\overline{\nabla \bullet V'\theta'}]$), where the horizontal eddy term is neglected when Eq. (1) is spatially averaged over a large area suitable for large-scale diagnostic analysis or over the GCE model if a cyclic lateral boundary condition is applied. The horizontal eddy term (entrainment and detrainment) could not be negligible over a small area or over the sub-domain averaged in this study.

Figures 5 and 6 illustrate each component of simulated heating structures associated with land and oceanic cases, respectively. These figures also show the characteristics of each heating component at specific stratifiorm amount (less than 5%) with different rainfall intensity (less than 20, between 80-100, 180-200, 380-400 and 480-500 mm/day) and at specific rainfall intensity (140-160 mm/day) with different stratiform amounts (less than 5, between 20-25, 45-50, 70-75 and 95-100%). These heating profiles are calculated over sub-domain (64 grids with 1 km spacing). Evident in the figures are: (1) latent heating is larger with large surface rainfall (Figs. 5a and 6a), (2) the level of heating maximum is higher with larger rainfall intensity (Figs. 5a and 6a), (3) a low level heating is evident for light rainfall (associated with shallow convective convection, Figs. 5a and 6a), (4) both eddy and radiative heating are quite smaller compared to heating but they cannot be negligible with light surface rainfall intensity (i.e., less than 100 mm/day, Figs. 5b, 5c, 5e, 5f, 6b, 6c, 6e and 6f), (5) the level of heating maximum is higher with less stratiform amount for oceanic case (Fig. 5d), (6) the cooling and heating aloft occurs at low troposphere with large stratiform amount with moderate rainfall (Figs, 5c and 6c). There are a few differences between land and ocean cases. For example, there are two heating maxima at low rainfall and small stratiform

amount for land case (Fig. 6a). The level of maximum heating is also higher for land case than oceanic case (Figs. 5a and 6a). In addition, the heating and eddy term is stronger for land case than oceanic case. This is because the convective vertical velocity is stronger for land case.

These GCE model simulated heating profiles are in many ways in good agreement with observed convective and stratiform heating structures (Johnson 1984; Houze 1989, 1997). These modeled convective and stratiform heating profiles will be in the new CSH algorithm's look-up table.

4. Performance of consistency check of new convective and stratiform heating algorithm

Current CSH algorithm uses surface precipitation rates and amount of stratiform rain. The CSH algorithm also utilizes a lookup table that consists of convective and stratiform diabatic heating profiles for various types of cloud systems in different geographic locations. These profiles stored in the lookup table are obtained from GCE model simulations or from budget calculations by temporally and spatially averaging the heating distributions in the convective and stratiform regions of the systems, which are then normalized by their total surface rainfall. Only about 15 heating profiles are in the current CSH heating algorithm. The improved CSH algorithm will also use the surface precipitation rates and amount of stratiform rain. The only difference is that much more heating profiles will be stored in the look-up table for improved CSH algorithm. These profiles will be selected based on the rainfall intensity and its stratiform amount. Some of heating profiles are shown in Figs 5 and

6 as discussed in Section 3.3 (only partially shown). In this section, the performance (including consistent check and comparison with previous CSH algorithm) of the improved CSH algorithm will be discussed.

4.1 Consistency Check

Consistency checking involving CRM-generated heating profiles and both algorithm-reconstructed and diagnostically-estimated heating profiles is a useful step in evaluating the performance of a given LH profile algorithm. In this process, the CRM simulation of a time-dependent precipitation process (multiple-day time series) is used to obtain the required input parameters for a given LH algorithm. The algorithm can then reconstruct the heating profiles that the CRM simulation originally produced, and finally both sets of conformal estimates (model and algorithm) can be compared to coincident estimates of diagnostically-based heating derived from radiosonde observations. Such observations from various field experiments, as well as simulations of individual precipitation systems, have been used for such consistency checks (Tao *et al.* 1990, 1993, 2000; Olson *et al.* 1999, 2006; Shige *et al.* 2004, 2006).

Figure 7 shows the time series of the GCE model simulated, new CSH reconstructed heating and sounding estimated heating for the SCSMEX case. For the CSH reconstructed heating is using the GCE model simulated surface rainfall and its stratiform percentage. Also only the heating associated with raining regions (or boxes) are retrieved. The results show that the pattern in temporal variations of the SLH algorithm-reconstructed heating profile agrees well with that of the GCE-simulated heating profile. The GCE model

simulated heating is stronger than sounding estimated. This is due to the fact that GCE simulated heating is based on five-minute cloud statistics (latent heating, eddy transport and radiative heating/cooling) compared to 3-hourly sounding estimates.

There are several differences between model simulated, CSH retrieved and sounding estimates. The CSH retrieved heating is generally slightly weaker than both simulated and sounding estimated. In addition, the retrieved heating structure does not show cooling due to the fact that the retrieved heating is only for raining region. There is no retrieved heating for those periods without surface rain (the radiative heating is much weaker than latent heating, see Fig. 5). Another major difference is the retrieved heating structure shows light heating above 10 km level (Steve and Xiping: Can we have explanation).

There are strong heating and cooling at upper troposphere simulated by the GCE model. It is mainly caused by the radiative processes. For example, a cloud emits infrared radiation at top upwards and absorbs the upward infrared radiation at bottom, which results in radiative cooling and heating at top and bottom, respectively. Since the heating at bottom increases instability and therefore large eddies there, the heating region is extended upwards. In contrast, the cooling at top increases instability and large eddies right below the cooling region, and thus the heating from eddies offsets the radiative cooling partly.

Forty four-day-averaged profile of the GCE model simulated, the CSH reconstructed and sounding estimated Q1 are shown in Fig. 8. These profiles are simply the time averages of the profiles shown in Fig. 7. The 44-day-averaged profiles of the reconstructed heating agree very well with the GCE simulated although the reconstructed heating is a little bit

weaker than the simulated one. The level of maximum heating simulated and reconstructed is about 7 km altitudes and is in good agreement with sounding estimated. Both simulated and reconstructed heating profiles have a distinct cooling near 4. km, which is due to the melting processes. This is because the eddy heat flux convergence compensates for the distinct cooling due to the melting. This feature is also shown in SLH reconstructed (see Shige *et al.* 2004). Both GCE simulated and CSH reconstructed is stronger than sounding estimate. Note that the model did not simulate strong cooling in middle and low troposphere between active convective events (Fig. 7).

4.2 Performance

The upper two panels of the **Fig. 9** illustrate 10-year mean apparent heating (Q_1) at two different altitudes (0.5, 4 and 7 km) over the global Tropics from the new CSH algorithm based upon the PR-monthly rainfall product. The new CSH algorithm has new heating look-up table that is binned based on rainfall intensity (mm/day) and stratiform amount (percentage). Then, the Q_1 profiles are calculated based on PR-retrieved surface rain rates and stratiform fractions at a grid scale of 0.5 degrees for either oceanic or continental locations. The concept between the new and old CSH algorithm is same. The only major difference between the new and old CSH algorithm is heating profile stored in the look-up table. The old CSH algorithm only consists of normalized convective/stratiform kernel profiles are created by averaging all 16 (4) oceanic (continental) base profiles in the CSH algorithm's complete library of 20 heating profile pairs distributed regionally and according to storm type. The new CSH algorithm consists more than 200 heating profiles in the oceanic and continental region, respectively.

As expected from the design of the CSH algorithm, the horizontal distribution of the estimated Q_1 structure is similar to the pattern of surface rainfall (lower panel of the Fig. 8). For example, well defined ITCZs in the east and central Pacific and Atlantic Oceans, a well-defined South Pacific Convergence Zone (SPCZ) in the central-southern Pacific Ocean, and broad areas of precipitation events spread over the continental regions are all evident. Also, strong LH release in the middle troposphere (5 ^{o}C day^{-1} and greater) is associated with heavier surface precipitation. Heating in the upper troposphere is weaker than those in the middle troposphere.

Figures 10(a) and 10(b) are the 10-year averaged Q1 derived from old and new CSH algorithm. Clearly, there are two heating maxima derived from both old and new CSH algorithm. Both occur about the same locations, and respond to the surface rainfall associated with the ITCZ (at 5^{o} North) in the North Hemisphere, and one associated with the SPCZ (2.5^{o} South). The heating is stronger in the North Hemisphere because the surface rainfall is larger in the North Hemisphere. This difference could have impact for large-scale circulation respond to the heating gradient between North and South Hemisphere. One major difference between old and new CSH algorithm is the new CSH retrieved stronger heating than that old CSH. The level of maximum of the heating is lower in the new CSH algorithm derived. Another major difference between old and new CSH algorithm is at the low troposphere. The heating at low troposphere is stronger in the new than old CSH algorithm near the equator.

Figure 10(c) shows the mean 10-year old and new CSH-retrieved average heating profile over the Tropics. The land and ocean components are also shown from both new and old CSH algorithm for comparison. There are very little variation of heating between land and ocean for old CSH CSH algorithm. For new CSH algorithm, the heating is much stronger between 2 and 8 km altitude over the land than over the ocean. The stronger convective heating in the land could be the consequences of stronger vertical velocity and / or large convective rain amount (Table 3). In addition, there is cooling at low troposphere in the new CSH over land. The drier environment in the land than the ocean could allow more evaporation cooling over the land region. Another major difference between new and old CSH algorithm is that level of maximum heating is lower (about 6 km altitude) for the new CSH algorithm.

Lin and Johnson (1996) compared the mean latent heating from the TOGA COARE, Marshall Islands region (Yanai *et al.* 1973) and the GATE region (Thompson *et al.* 1979). Their results show that the level of maximum heating is about 6 – 6.5 km altitude for the Western Pacific (TOGA COARE and Marshall Island region), but is only about 4 km altitude for the GATE region. The lower level of maximum heating the GATE region may be due to lower SST in eastern Atlantic (Thompson *et al.* 1979). Greco *et al.* (1994) calculated latent heating profiles over S. America from the sounding network network. Their results indicated that the distribution of heating is quite similar to the studies of those of West African squall lines (Chong and Hauser 1990). Peak heating also occurs between 500 and 550 hPa (about 5-6 km). The new CSH algorithm retrieved level of the maximum heating is also about 6 km altitude that is in good agreement with these diagnostic studies. However, the level of the maximum heating is higher (about 7.5 km) for monsoon over S. China Sea (SCSMEX

NESA, Johnson and Ciesielski, 2002) and for convective system over S. America (LBA, Halverson *et al.* 2002). The regional analyses of the new CSH products including comparison with diagnostic studies and with other heating products (i.e., products derived from other heating algorithms, SLH and TRAIN) will be conducted in next paper.

5. Summary

The relationship between rainfall intensity and stratiform cloud was examined by analyzing TRMM PR and GCE model simulated results. The relationship between surface rainfall intensity, stratiform percentage and latent heating was also examined by using GCE model simulated precipitation processes. These results were used for improving the CSH algorithm. The performance of the new CSH algorithm was presented by comparing the results with previous CSH algorithm. The major highlights are as follows:

- Both PR estimated and GCE model simulated results showed that are more stratiform rain amount for light rain for both ocean and land region, but more convective rain amount for heavy rainfall. The differences between oceanic and land region is that more convective rain for precipitation rate over 100 mm/day for the land region than its oceanic counterpart.

- One major difference between PR and GCE simulated rain intensity and stratiform relationship is in very light (less than 10 mm/day) rainfall region. This difference is caused by the PR sensitivity (17 dBz) on light rainfall.

- The GCE model simulated the stratiform percentage is in excellent agreement with PR estimated for SCSMEX (1998) and ARM (2002) cases. But the GCE simulated more rainfall

amount for ARM case compared to PR estimated. On the other hand, the GCE model simulated rainfall amount is in good agreement with sounding estimated. Sampling is the main cause for the difference between PR estimated and GCE model simulated rainfall amount.

- Each component and profile (latent heat, eddy term and radiative/cooling/heating) of Q1 associated different stratiform percentage and rainfall intensity for land and ocean cases, was simulated by GCE model. These profiles are used for new CSH algorithm's look-up tables. There are many similarities in these profiles between land ocean cases. For example: (1) latent heating is larger with large surface rainfall, (2) the level of heating maximum is higher with larger rainfall intensity, (3) a low level heating is evident for light rainfall, (4) both eddy and radiative heating/cooling are quite smaller compared to heating but they cannot be negligible with light surface rainfall intensity, and (5) the cooling and heating aloft occurs at low troposphere with large stratiform amount with moderate rainfall. The major differences are that there are two heating maxima at low rainfall and small stratiform amount for land case and the level of maximum heating is also higher for land case than oceanic case. In addition, the heating and eddy term is stronger for land case than oceanic case.

- One major difference between new and old CSH algorithm is that the level of maximum heating is 1 to 1.5 km lower for the new than old CSH algorithm. Another major difference is that there is more variation in heating profiles in the ocean and land regions. For old CSH algorithm retrieved heating: there is almost no variation of heating between land and ocean for old CSH algorithm.

The results from this paper are two-dimensional version of GCE model was used to provide the heating profiles for CSH algorithm. It is known that the results from 2D and 3D CRM simulations can differ not only in cloud dynamics but also microphysics (i.e., Tao *et al.* 1986; Johnson *et al.* 2002; and Zeng *et al.* 2008). More convective cores with stronger vertical velocity exist in a 3D CRM than in a 2D one. As a result, the cloud ice content in the upper troposphere in a 3D CRM is higher than that in its 2D counterpart (Zeng et al. 2008). The sensitivity of the relationship between rainfall intensity and its stratiform amount using 3D needs to be examined.

Only limited CRM simulated cases were used in this study. The Observations from additional field experiments (TWP-ICE, GAME and future GPM Ground Validation (GV) site) will be needed to provide new types of initial conditions for GCE model. In addition, the large scale analyses (i.e. NASA Goddard Modern era retrospective-analysis for research and applications, MERRA) could also provide initial and condition and forcing for CRM. Figure 10 shows the preliminary results using MERRA to provide the forcing for GCD model. The results indicate that the GCE+MERRA approach can provide reasonably good simulations of reality. The two simulations generally agree with each other to a large extent. Thus, the GCE+MERRA, are compatible and could be used for additional cases (especially for those regions with large surface rainfall, such as Indian Ocean, SPCZ, S. America, and Africa) for CSH algorithm.

6. Acknowledgements

This research was supported by the NASA Headquarters Atmospheric Dynamics and Thermodynamics Program and the NASA Precipitation Measuring Mission (PMM). The authors are grateful to Dr. R. Kakar at NASA headquarters for his support of this research. Acknowledgment is also made to the NASA Goddard Space Flight Center and NASA Ames for computer time used in this research.

References

Das, S., D. Johnson and W.-K. Tao, 1999: Single-column and cloud ensemble model simulations of TOGA COARE convective systems, *J. Meteor. Soc. Japan*, 77, 803-826.

Chong, M. and D. Hauser, 1990: A tropical squall line observed during the COPT 81 experiment in West Africa. Part III: Heat and moisture budgets. *Mon. Wea. Rev.*, **118**, 1696-1706.

Gamache, J. F., and R. A. Houze, Jr., 1983: Water budget of a mesoscale convective system in the tropics. *J. Atmos. Sci.*, **40**, 1835-1850.

Greco, S., J. Scala, J. Halverson, H. L. Massie, W.-K. Tao, and M. Garstang, 1994: Amazon coastal squall lines. Part II: Heat and moisture transports. *Mon. Wea. Rev.*, **122**, 623-635.

Grecu, M. W. Olson, C.-L. Shie, T. L'Ecuyer, and W.-K. Tao, 2009: Combining Satellite Microwave Radiometer and Radar Observations to Estimate Atmospheric Latent Heating Profiles. *J. Climate* (submitted).

Halverson, J.B., T. Rickenbach, B. Roy, H. Pierce, and E. Williams, 2002: Environmental characteristics of convective systems during TRMM-LBA. *Mon. Wea. Rev.*, **130**, 1493–1509.

Houze, R. A., Jr., 1977: Structure and dynamics of a tropical squall-line system. *Mon. Wea. Rev.*, 105, 1540-1567.

Houze, R.A., Jr., 1982: Cloud clusters and large-scale vertical motions in the tropics. *J. Meteor. Soc. Japan*, **60**, 396-409.

Houze, R.A., Jr., 1997: Stratiform precipitation in regions of convection: A meteorological paradox. *Bull. Amer. Meteor. Soc.*, **78**, 2179-2196.

Johnson, R.H., 1984: Partitioning tropical heat and moisture budgets into cumulus and mesoscale components: Implication for cumulus parameterization. *Mon. Wea. Rev.*, **112**, 1656-1665.

Johnson, R. H. and P. J. Hamilton, 1988: The relationship of surface pressures to the precipitation and airflow structure of an intense midlatitude squall line. *Mon. Wea. Rev.*, **116**, 1444-1471.

Johnson, R. H., and P. E. Ciesielski, 2002: Characteristics of the 1998 summer monsoon onset over the northern south China sea. *J. Meteor. Soc. Japan*, **80**, 561-578.

Johnson, D. E., W.-K. Tao, J. Simpson, and C.-H. Sui, 2002: A study of the response of deep tropical clouds to large-scale thermodynamic forcing. Part I: Modeling strategies and simulations of TOGA COARE convective systems. *J. Atmos. Sci.*, **59**, 3492-3518.

Katsumata, M., S. Mori, T. Ushiyama, Y.-M. Kodama, S. Satoh, 2009: An improved version of the PRH latent heating estimation algorithm based on the observed vertical structure. *J. Climate* (submitted).

Klemp, J. B. and R. B. Wilhelmson, 1978: The simulation of three-dimensional convective storm dynamics. *J. Atmos. Sci.*, **35**, 1070-1096.

Lang, S., W.-K. Tao, J. Simpson, and B. Ferrier (2003), Modeling of convective-stratiform precipitation processes: Sensitivity to partitioning methods. *J. Appl. Meteor.,* **42**, 505-527.

Li, X., C.-H. Sui, K.-M. Lau, and M.-D. Chou, 1999: Large-scale forcing and cloud-radiation interaction in the tropical deep convective regime. *J. Atmos. Sci.*, **56**, 3028-3042.

Lin, X., and R. H. Johnson, 1996: Heating, moistening and rainfall over the western Pacific during TOGA COARE. *J. Atmos. Sci.*, 53, 3367-3383.

Lin, Y.-L., R. D. Farley, and H. D. Orville, 1983: Bulk parameterization of the snow field in a cloud model. *J. Clim. Appl. Met.*, **22**, 1065-1092.

Olson, W.S., C.D. Kummerow, Y. Hong, and W.-K. Tao, 1999: Atmospheric latent heating distributions in the tropics derived from passive microwave radiometer measurements. *J. Appl. Meteor.*, **38**, 633-664.

Olson, W.-S., C. D. Kummerow,, S. Yang, G. W. Petty, W.-K. Tao, T. L. Bell, S. A. Braun, Y. Wang, S. E. Lang, D. E. Johnson and C. Chiu, 2006: Precipitation and latent heating distributions from satellite passive microwave radiometry Part I: Method and uncertainties. *J. Applied Meteor.*, **45**, 702-720.

Rutledge, S. A. and P. V. Hobbs, 1984: The mesoscale and microscale structure and organization of clouds and precipitation in mid-latitude clouds. Part XII: A diagnostic

modeling study of precipitation development in narrow cold frontal rainbands. *J. Atmos. Sci.*, **41**, 2949-2972.

Rutledge, S. A., and R. A. Houze, Jr., 1987: A diagnostic modeling study of the trailing stratiform of a midlatitude squall line. *J. Atmos. Sci.*, **44**, 2640-2656.

Satoh, S., and A. Noda, 2001: Retrieval of latent heating profiles from TRMM radar data. Proceedings of 30th International Conf. on Radar Meteorology, [Munich, Germany; 19-24 July 2001], 340-342.

Satoh, S., A. T. Noda, and T. Iguchi, 2009: Retrieval of latent heating profiles in various cloud systems from TRMM PR data. *J. Meteor. Soc. Japan,* (submitted).

Schumacher, C., and R. A. Houze, Jr., 2003: Stratiform rain in the tropics as seen by the TRMM Precipitation Radar. J. Climate, 16, 1739-1756.

Schumacher, C., R.A. Houze, Jr., and I. Kraucunas, 2004: The tropical dynamical response to latent heating estimates derived from the TRMM precipitation radar. *J. Atmos. Sci.*, **61**, 1341-1358.

Shige, S., Y. N. Takayabu, **W**.-K. Tao and C.-L. Shie, 2007: Spectral retrieved of latent heating profiles from TRMM PR data. Part II: Algorithm improvement and its estimates over the tropical ocean regions. *J. Applied Meteor.* **46**, 1098-1124.

Shige, S., Y. N. Takayabu, S. Kida, W.-K. Tao, X. Zeng and T. L'Ecuyer, 2009: Spectral retrieved of latent heating profiles from TRMM PR data. Part IV: Comparisons of lookup tables from two- and three-dimensional simulations. *J. Climate* (submitted).

Shige, S., Y. N. Takayabu, and W.-K. Tao, 2008: Spectral retrieved of latent heating profiles from TRMM PR data. Part III: Moistening estimates over the tropical ocean regions. *J. Applied Meteor. Climatol.* **47**, 620-640.

Simpson, J. and W.-K. Tao, 1993: The Goddard Cumulus Ensemble Model. Part II: Applications for studying cloud precipitating processes and for NASA TRMM. *Terrestrial, Atmospheric and Oceanic Sciences*, **4**, 73-116.

Smith, E.A., X. Xiang, A. Mugnai, and G. Tripoli, 1992: A cloud radiation model for spaceborne precipitation retrieval. *Extended Abstract Vol. of International TRMM Workshop on the Processing and Utilization of the Rainfall Data Measured from Space*, Communications Research Laboratory, Tokyo, Japan, 273-283.

Smith, E.A., X. Xiang, A. Mugnai, and G.J. Tripoli, 1994a: Design of an inversion-based precipitation profile retrieval algorithm using an explicit cloud model for initial guess microphysics. *Meteorol. Atmos. Phys.*, **54**, 53-78.

Smith, E., W.-K., Tao, Z. S. Haddad, A. Hou, R. Kakar, M. Katsumata, T. N. Krishnmurti, S. Lang, W. S. Olson, S. Satoh, S. Shige, Y. Takayabu, G. Tripoli, and S. Yang 2008: A

Review of TRMM Satellite Latent Heat Retrieval: Algorithm Development, Validation and Applications. *Special Issue on Satellite Precipitation Observation, J. Meteor. Soc. Japan,* (submitted).

Smolarkiewicz, P. K., and W. W. Grabowski, 1990: The multidimensional positive advection transport algorithm: non-oscillatory option. *J. Comp. Phys.*, **86**, 355-375.

Soong, S.-T. and Y. Ogura, 1980: Response of trade-wind cumuli to large-scale processes. *J. Atmos. Sci.*, **37**, 2035-2050.

Soong, S.-T., and W.-K. Tao (1980), Response of deep tropical clouds to mesoscale processes. *J. Atmos. Sci.*, **37**, 2016-2036.

Starr, D. O., and S. K. Cox, 1985: Cirrus clouds. Part I: cirrus cloud model. *J. Atmos. Sci.*, **42**, 2663-2681.

Sui, C.-H., and M. Yanai, 1986: Cumulus ensemble on the large-scale vorticity and momentum fields of GATE. Part I: Observational evidence. *J. Atmos. Sci.*, **43**, 1618-1642.

Tao, W.-K., and S.-T. Soong (1986) A study of the response of deep tropical clouds to mesoscale processes: Three-dimensional numerical experiments. *J. Atmos. Sci.*, **43**, 2653-2676.

Tao, W.-K., J. Simpson, and S.-T. Soong (1987), Statistical properties of a cloud ensemble: A numerical study. *J. Atmos. Sci.*, **44**, 3175-3187.

Tao, W.-K., J. Simpson, S. Lang, M. McCumber, R. Adler, and R. Penc, 1990: An algorithm to estimate the heating budget from vertical hydrometeor profiles. *J. Appl. Meteor.*, **29**, 1232-1244.

Tao, W.-K. and J. Simpson, 1993: The Goddard Cumulus Ensemble model. Part I: Model description. *Terr. Atmos. Oceanic Sci.*, **4**, 19-54.

Tao, W.-K., S. Lang, J. Simpson, and R. Adler, 1993: Retrieval algorithms for estimating the vertical profiles of latent heat release: Their applications for TRMM. *J. Meteor. Soc. Japan*, **71**, 685-700.

Tao, W.-K., J. Simpson, C.-H. Sui, B. Ferrier, S. Lang, J. Scala, M.-D. Chou, and K. Pickering (1993), Heating, moisture and water budgets of tropical and mid-latitude squall lines: Comparisons and sensitivity to longwave radiation. *J. Atmos. Sci.*, **50**, 673-690

Tao, W.-K., S. Lang, J. Simpson, C.-H. Sui, B. Ferrier, and M.-D. Chou, 1996: Mechanism of cloud-radiation interaction in the tropics and mid-latitude. *J. Atmos. Sci.*, **53**, 2624-2651.

Tao, W.-K., S. Lang, J. Simpson, W.S. Olson, D. Johnson, B. Ferrier, C. Kummerow, and R. Adler, 2000: Retrieving vertical profiles of latent heat release in TOGA COARE convective systems using a cloud resolving model, SSM/I and radar data. *J. Meteor. Soc. Japan,* **78**, 333-355.

Tao, W.-K., S. Lang, W.S. Olson, S. Yang, R. Meneghini, J. Simpson, C. Kummerow, E. Smith and J. Halverson, 2001: Retrieved vertical profiles of latent heating release using TRMM rainfall products for February 1998. *J. Appl. Meteor.,* **40**, 957-982.

Tao, W.-K., 2003: Goddard Cumulus Ensemble (GCE) Model: Application for understanding precipitation processes. *AMS Meteorological Monographs*: *Cloud Systems, Hurricanes, and the Tropical Rainfall Measuring Mission (TRMM) -- A Tribute to Dr. Joanne Simpson*, **29**, 107-138.

Tao, W.-K., J. Simpson, D. Baker, S. Braun, M.D. Chou, B. Ferrier, D. Johson, A. Khain, S. Lang, B. Lynn, C.-L Shie, D. Starr, Y. Wang, and P. Wetzel, 2003a: Microphysics, radiation and surface processes in the Goddard Cumulus Ensemble (GEC) model. *Meteorol. Atmos. Phys*., **82**, 97-137.

Tao, W.-K., C.-L. Shie, R. Johnson, S. Braun, J. Simpson, and P.E. Ciesielski, 2003b: Convective systems over the South China Sea: Cloud resolving model simulations. *J. Atmos. Sci.,* **60**, 2929-2956.

Tao, W.-K., D. Johnson, C.-L. Shie, and J. Simpson. 2004: Atmospheric energy budget and large-scale precipitation efficiency of convective systems during TOGA COARE, GATE, SCSMEX and ARM: Cloud-resolving model simulations, *J. Atmos. Sci*., **61**, 2405-2423.

Tao, W.-K., E.A. Smith, R.F. Adler, Z.S. Haddad, A.Y. Hou, T. Iguchi, R. Kakar, T.N. Krishnamurti, C.D. Kummerow, S. Lang, R. Meneghini, K. Nakamura, T. Nakazawa, K. Okamoto, W.S. Olson, S. Satoh, S. Shige, J. Simpson, Y. Takayabu, G.J. Tripoli, and S. Yang, 2006: Retrieval of latent heating from TRMM measurements. *Bull. Amer. Meteor. Soc.,* **87,** 1555-1572.

Tao, W.-K., R. Houze, Jr., and E. Smith, 2007: Summary of the 4th TRMM Latent Heating Workshop, *Bull. Amer. Meteor. Soc.,* **88**, 1255, 1259.

Thompson, R. M., Jr., S. W. Payne, E. E. Recker, and R. J. Reed, 1979: Structure and properties of synoptic-scale wave disturbances in the intertropical convergence zone of the eastern Atlantic. *J. Atmos. Sci*., **36**, 53-72.

Xu, K.-M., R. T. Cederwall, L. J. Donner, F. Guichard, W. W. Grabowski, D. E. Johnson, M. Khairoutdinov, S. K. Krueger, J. C. Petch, D. A. Randall, C. J. Seman, W.-K. Tao, S. Xie, J. Jio and M.-H. Zhang, 2002: Iintercomparison of cloud-resolving models with the ARM Summer 1997 IOP data *Q. J. R. Met. Soc.,* 128, 593-624.

Wang, Y., W.-K. Tao, and J. Simpson, 1996: The impact of a surface layer on a TOGA-COARE cloud system development. *Mon. Wea. Rev.*, **124**, 2753-2763.

Yanai, M., S. Esbensen, and J. Chu, 1973: Determination of average bulk properties of tropical cloud clusters from large-scale heat and moisture budgets. *J. Atmos. Sci.*, **30**, 611-627.

Yang, S., and E.A. Smith, 1999b: Four dimensional structure of monthly latent heating derived from SSM/I satellite measurements. *J. Clim.*, **12**, 1016-1037.

Yang, S., W.S. Olson, J.-J. Wang, T.L. Bell, E.A. Smith, and C.D. Kummerow, 2006: Precipitation and latent heating distributions from satellite passive microwave radiometry. Part II: Evaluation of estimates using independent data. *J. Appl. Meteor.*, 45, 721-739.

Zhang, M. H. and J. L. Lin, 1997: Constrained variational analysis of sounding data bases on column-integrated budgets of mass, heat, moisture, and momentum: Approach and application to ARM measurements. *J. Atmos. Sci.*, **54**, 1503-1524.

Zhang, M. H., J. L. Lin, R. T. Cederwall, J. J. Yio, and S. C. Xie, 2001: Objective analysis of ARM IOP Data: Method and sensitivity. *Mon. Wea. Rev.*, **129**, 295-311.

Zeng, X., W.-K. Tao, M. Zhang, S. Lang, C. Peters-Lidard, J. Simpson, S. Xie, S. Kumar, J. V. Geiger, C.-L. Shie, and J. L.. Eastman (2007), Evaluation of long-term cloud-resolving modeling with observational cloud data. *J. Atmos. Sci.,* **64**, 4153-4177.

Zeng, X., W.-K. Tao, S. Lang, A. Hou, M. Zhang, and J. Simpson, 2008: On the sensitivity of Atmospheric ensemble to cloud microphysics in long-term cloud-resolving model simulations. *J. Meteor. Soc. Japan*, *Special Issue on high-resolution cloud models*, **86A**, 45-65.

Zeng, X., W.-K. Tao, M.-H. Zhang, A. Y. Hou, S. Xie, S. Lang, X. Li, D. O'C Starr and X. Li, 2009:A contribution by ice nucli to global warming. *Quart. J. Roy. Meteor. Soc.* **(accepted).**

Zipser, E. J., R. J. Meitin, and M. A. LeMone, 1981: Mesoscale motion fields associated with a slowly moving GATE convective band. *J. Atmos. Sci.*, **38**, 1725-1750.

	TRMM Data Needed	Heating Products	Key References in Algorithm description
CSH (Convective-Stratiform Heating)	PR, TMI, PR-TMI	Q_1, LH	Tao *et al.* (1993; 2000; 2001)
SLH (Spectral Latent Heating)	PR	LH, Q_1-Q_R	Shige *et al.* (2004; 2007, 2009)
TRAIN (Trained radiometer algorithm)	TMI (PR Training)	Q_1-Q_R, LH	Grecu and Olson (2006), Olson *et al.* (2006), Grecu *et al.* (2009)
HH (Hydrometeor Heating)	PR-TMI	LH	Yang *et al.* (1999; 2006)
PRH (Precipitation Radar Heating)	PR	LH	Satoh and Noda (2001), Katsumata *et al.* (2009)

Table 1 *Summary of the five LH algorithms participating. Data inputs, retrieved products, and salient references included. Note conventional relationship between Q_1 (apparent heat source), LH, and Q_R (radiative heating) is expressed by Q_1-Q_R = LH + EHT, where the final term represents eddy heat transport by clouds (noting that vertically integrated EHT is zero, i.e., it provides no explicit influence on surface rainfall). Note that CSH, SLH and TRAIN explicitly used the CRM simulated latent heating profiles as their heating algorithm - look up tables. Both HH and PRH also applied implicitly CRM simulated results (i.e., cloud vertical velocity).*

Field Campaign	*Geographic Location*	*Starting Date*	*Modeling Days*	
ARM-SGP-97	(37°N, 97°W)	18 Jun 1997	29	Tao *et al.* (2004); Zeng *et al.* (2009)
ARM-SGP-02		25 May 2002	20	Zeng *et al.* (2007, 2009)
SCSMEX/NESA	(21°N, 117°E)	6 May 1998	44	Tao *et al.* (2003), Zeng *et al.* (2008)
TOGA-COARE	(2°S, 154°E)	1 Nov 1992	61	Das *et al.* (1999); Johnson *et al.* (2002); Zeng *et al.* (2009)
GATE	(9°N, 24°W)	1 Sep 1974	18	Li *et al.* (200x); Zeng *et al.* (2009)

Table 2 Field campaigns (ARM, SCSMEX, TOGA COARE and GATE) including the geographic location, starting time and integration length of GCE model simulations. Also include the previous GCE modeling papers that have simulated the case.

	Rainfall amount (mm/day)	Stratiform Percentage (%)
Global Tropics	2.26	52.8
Ocean	2.35	55.0
Land	2.06	47.4
SCSMEX (1998)	11.24	42.3
SCSMEX (10 years)	3.64	49.8
ARM (2002)	2.59	35.7
ARM (10 years)	2.36	41.1

Table 3 PR estimated rainfall amount and stratiform % (Global, Land, Oceans, SCSMEX (1998), SCSMEX (10 year), ARM (1997, 2000) and ARM (10 year))

	Simulated Rainfall amount (mm/day)	Stratiform Percentage (%)	Estimated Rainfall amount (mm/day)
SCSMEX	12.31	42.6	11.35
ARM (1997)	4.31	41.3	4.32
ARM (2002)	4.85	36.0	4.77
TOGA COARE (1992-1993)	7.72	47.6	9.32
GATE (1974)	10.56	41.4	11.38

Table 4 CRM simulated rainfall amount and stratiform % (SCSMEX (1998), ARM (1997, 2002), TOGA COARE (1992) and GATE (1974))

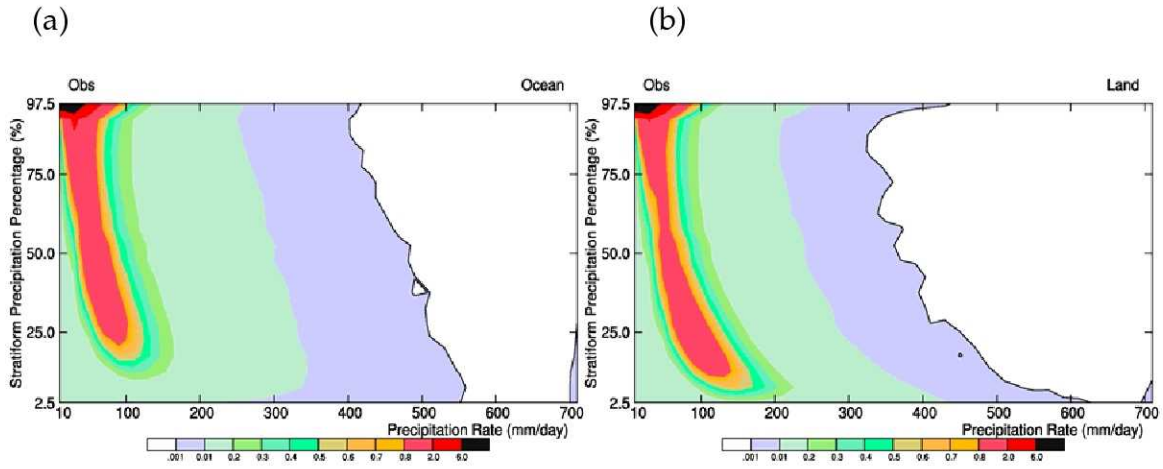

Fig. 1 Hit frequency of the TRMM observations over **(a)** oceanic and **(b)** continental regions.

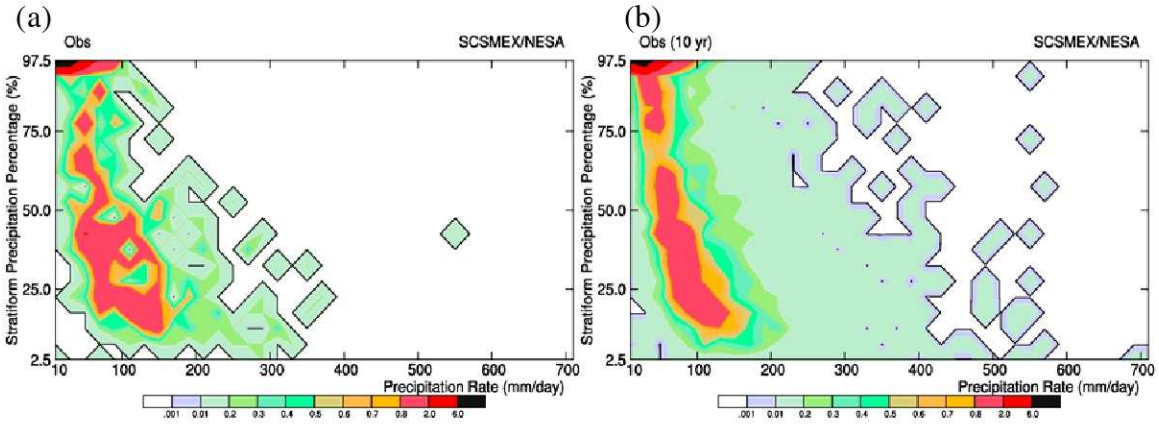

Fig. 2 **(a)** The same as Fig. 1 except for TRMM observations over SCSMEX/NESA for May-June of 1998. **(b)** as **(a)** except for 10 years of observations.

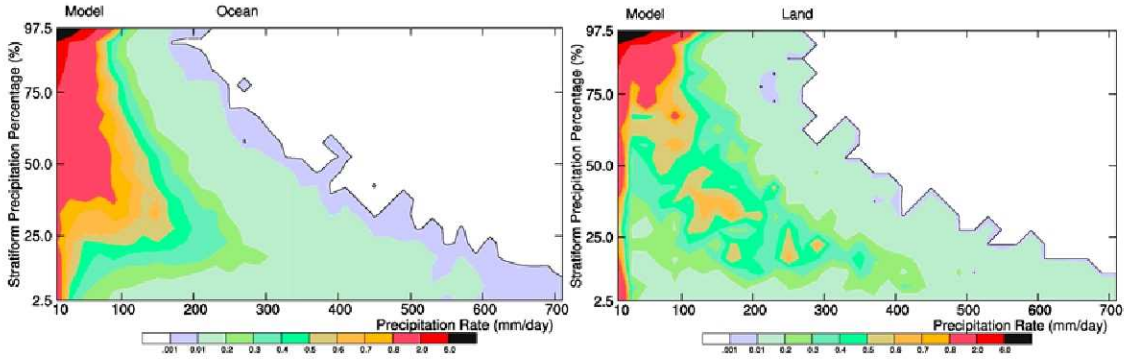

Fig. 3 Same as Fig. 2 except for GCE model simulation. **(a)** is for oceanic (TOGA COARE, GATE and SCSMEX) case and (**b**) is for continental (ARM 1997 and 2002) case.

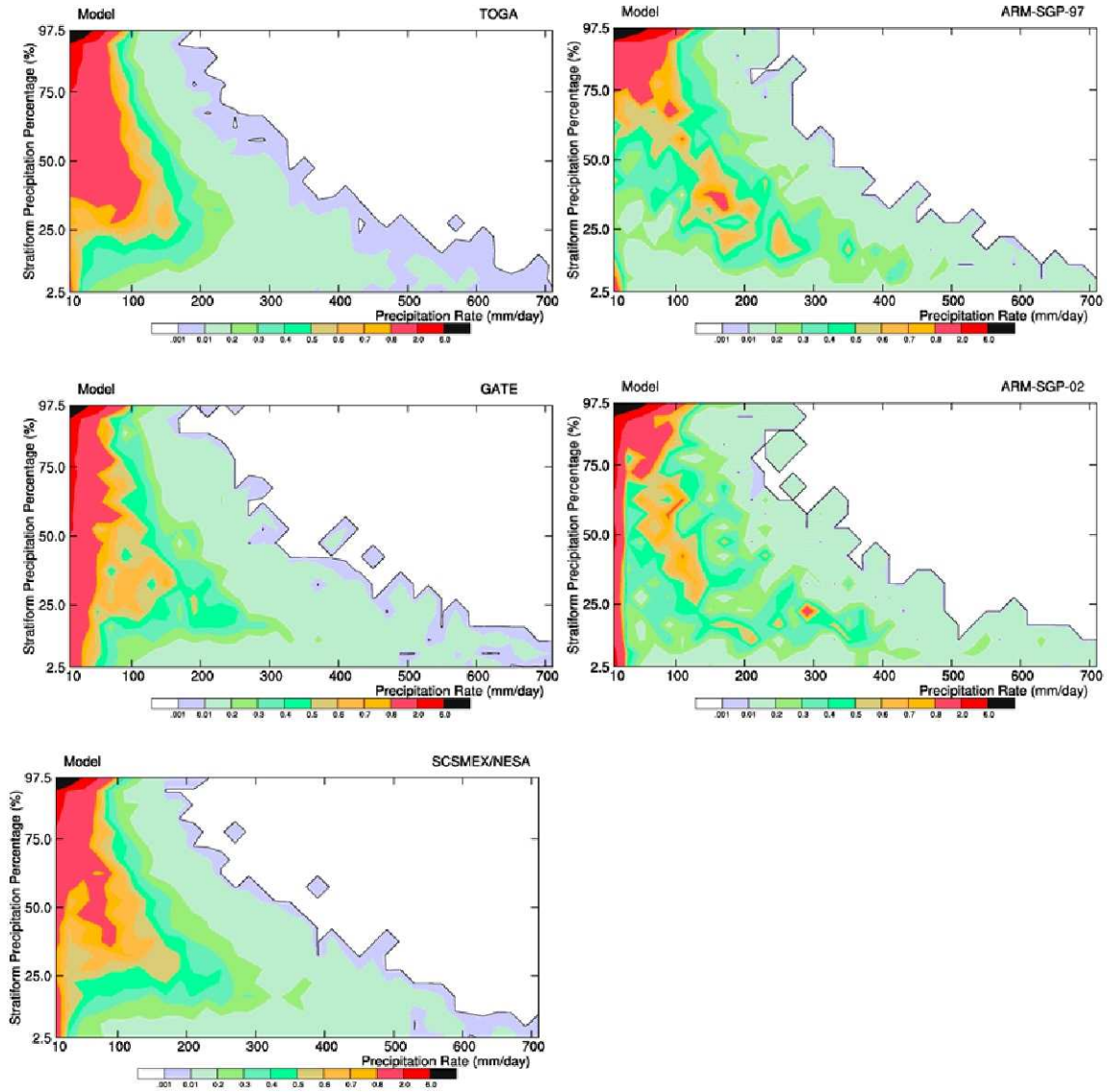

Fig. 4 Same as Fig. 2 except for GCE model simulation. Left three panels are oceanic cases, TOGA COARE, GATE and SCSMEX. Right two panels are continental cases, ARM 1997 and 2002.

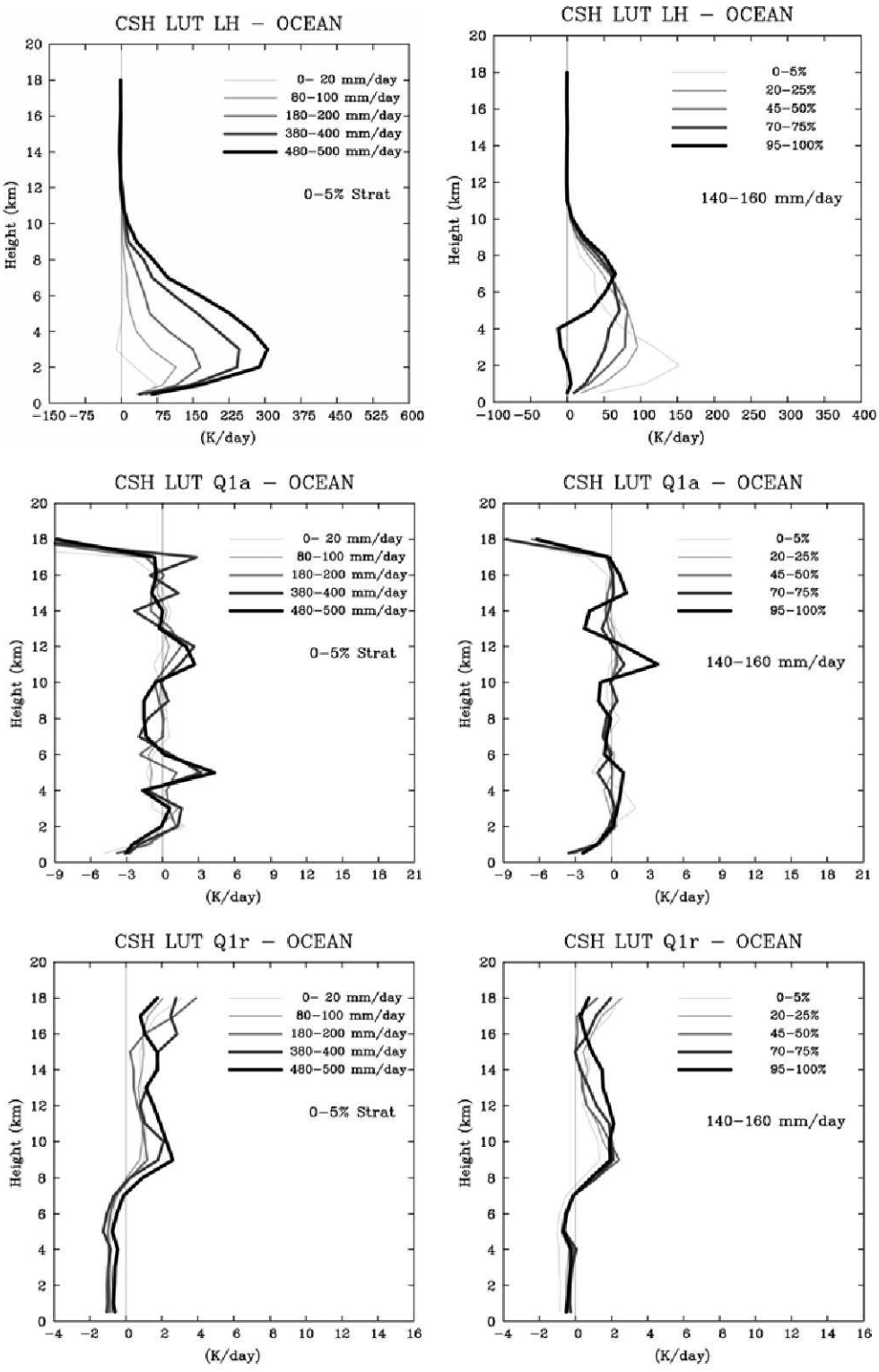

Fig. 5 Vertical profiles of the latent heating rate (top), eddy rate (middle) and radiative rate (bottom). Line labels indicate the range of the convective precipitation percentage.

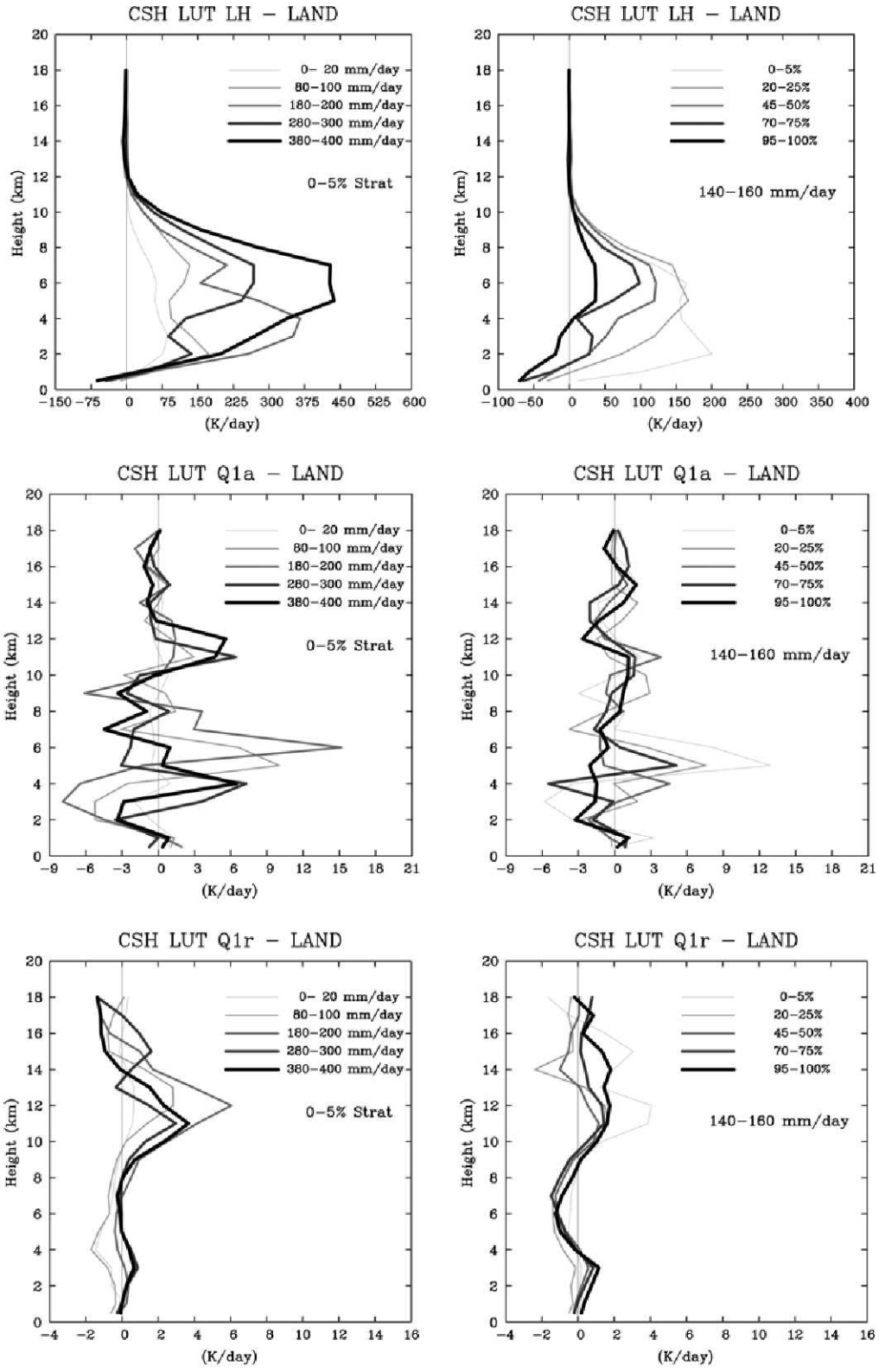

Fig. 6 The same as Fig. 5 except for land case.

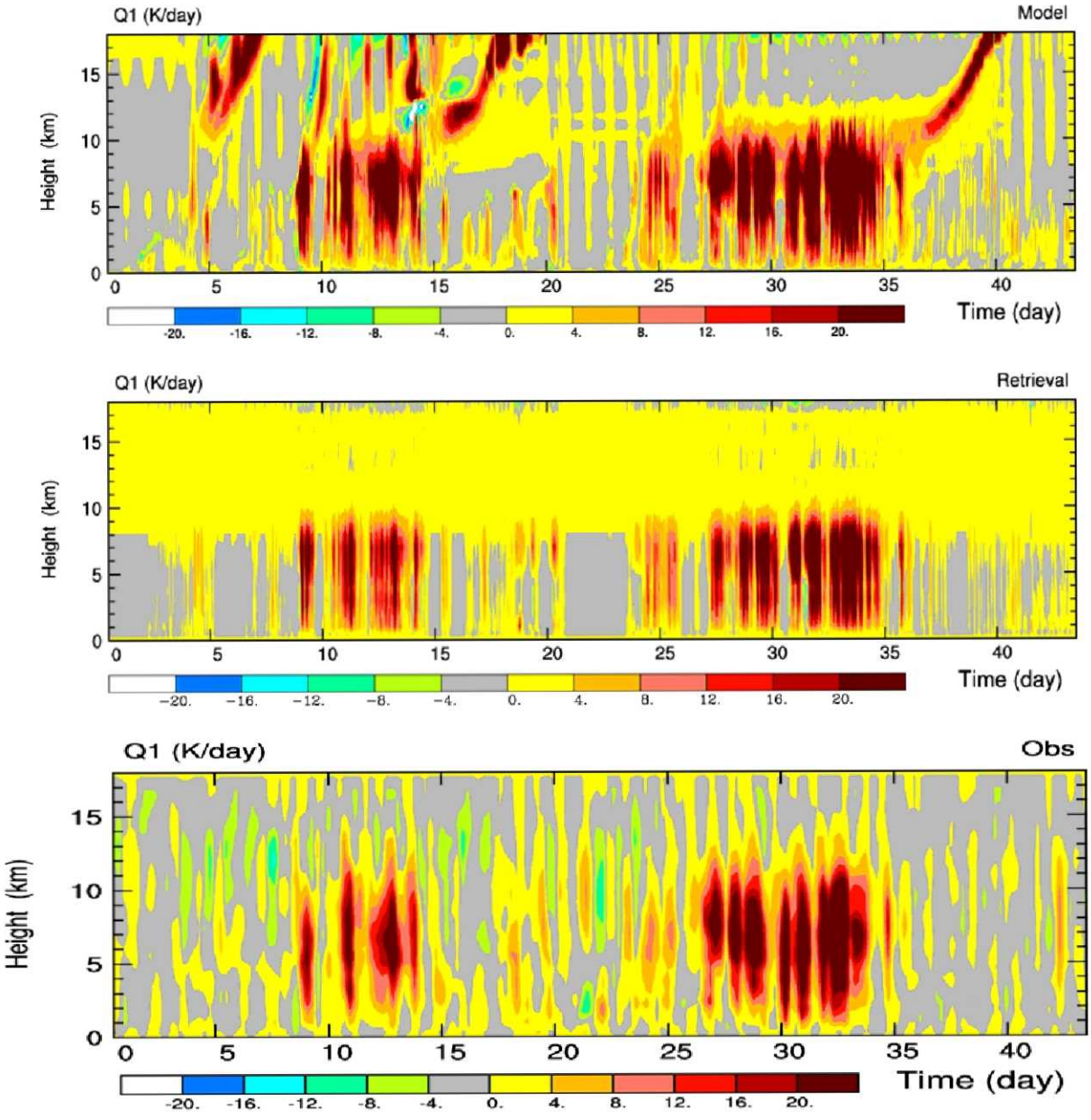

Fig. 7 Time-height cross sections of the modeled (top), retrieved (middle) and observed (bottom) Q1 in SCSMEX/NESA case.

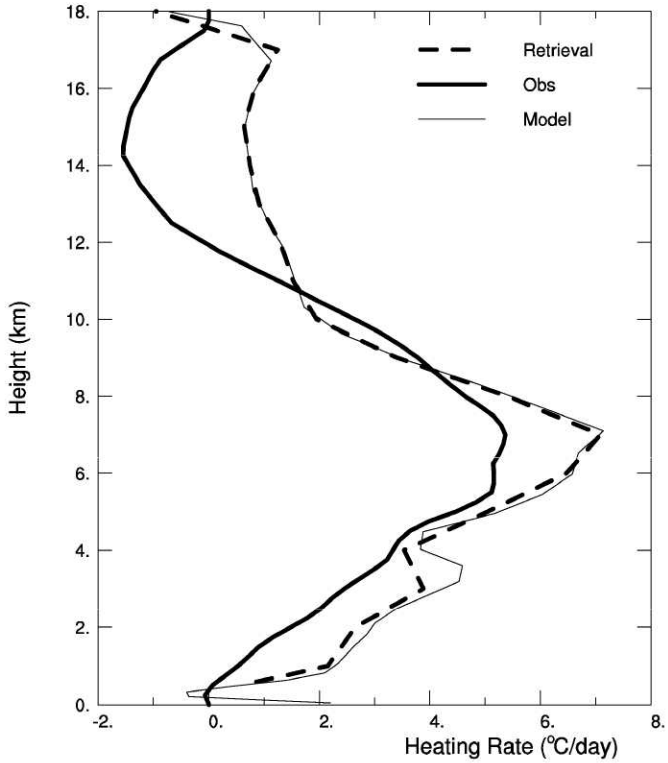

Fig. 8 Vertical profiles of mean Q1 over SCSMEX/NESA that is observed (thick solid), modeled (thin solid), retrieved (thick dashed line).

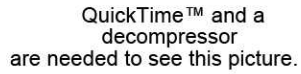

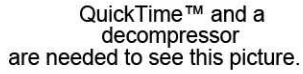

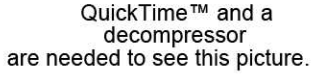

Fig. 9 Ten-year mean *Q1* heating rates at 7, 3, and 1 km AGL (upper 3 panels) along with surface rain rates (lower panel) over the global Tropics determined by the Goddard Space Flight Center (GSFC) Convective-Stratiform Heating (CSH) algorithm applied to 1998-2002 Precipitation Radar (PR) measurements acquired from the Tropical Rainfall Measuring Mission (TRMM) satellite

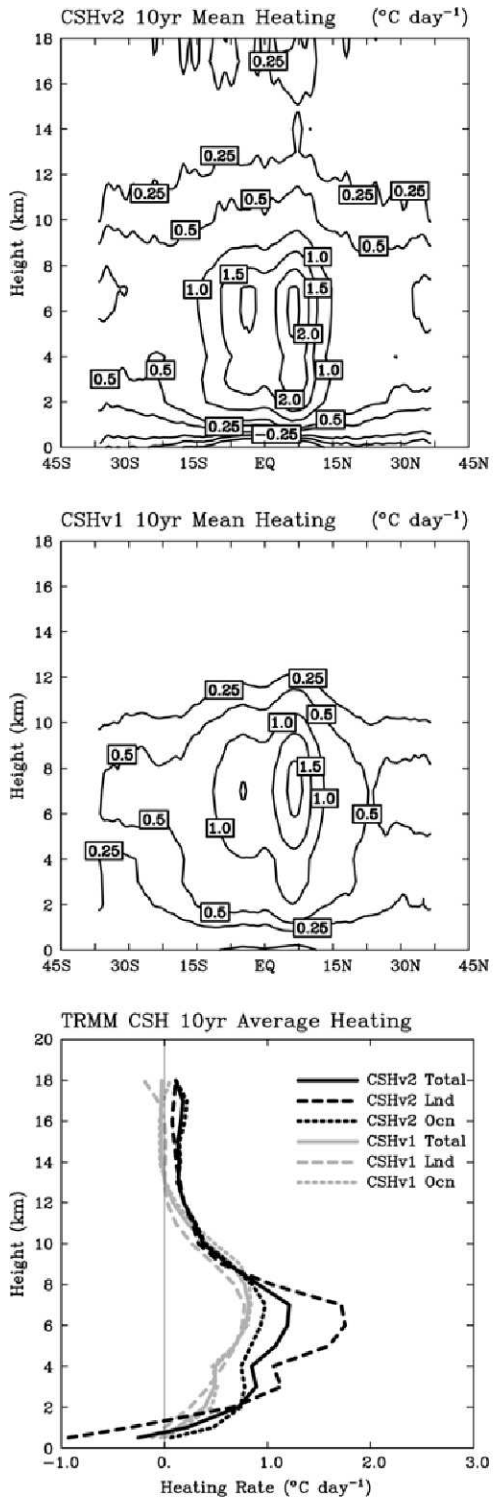

Fig. 10 Zonal distribution of heating structure from new (top) and old (middle) CSH algorithm. The bottom shows the global averaged heating profiles (including land and ocean component using new and old CSH algorithm).

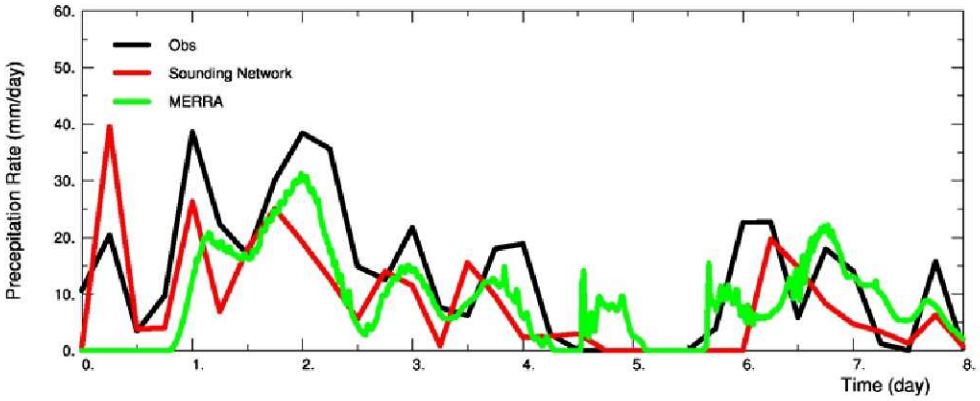

Fig. 11 The bold black line is the 3-hourly time series of domain-averaged precipitation observed during SCSMEX period (from 0600 UTC 18 May to 0600 UTC 26 May 1998). The red line is the 3-hourly precipitation time series from GCE simulation driven by SCSMEX intensively observed large-scale tendencies. The green line is same to the red line except the GCE was driven by tendencies from MERRA output. The two simulations generally agree with each other to a large extent and it indicates that the GCE+MERRA approach can provide reasonably good simulations of reality.